Journal of Catalysis **196,** 158–166 (2000)
doi:10.1006/jcat.2000.3031, available online at http://www.idealibrary.com on IDEAL®

Synthesis of Zeolite ZSM-57 and Its Catalytic Evaluation for the 1-Butene Skeletal Isomerization and *n*-Octane Cracking

Song-Ho Lee,* Dong-Koo Lee,* Chae-Ho Shin,*,[1] Woon Chang Paik,† Won Mook Lee,† and Suk Bong Hong†,[1]

*Department of Chemical Engineering, Chungbuk National University, Chungbuk 361-763, Korea; and †School of Chemical Engineering and Technology, Taejon National University of Technology, Taejon 305-719, Korea

Received May 15, 2000; revised August 7, 2000; accepted August 7, 2000

The synthesis of the medium-pore zeolite ZSM-57 in the presence of sodium and *N,N,N,N′,N′,N′*-hexaethylpentanediammonium cations is described. Under the synthesis conditions studied here, crystallization of pure ZSM-57 was possible only from synthesis mixtures with a very narrow range of SiO_2/Al_2O_3 and $NaOH/SiO_2$ ratios. The catalytic properties of H-ZSM-57 are evaluated for the skeletal isomerization of 1-butene to isobutene and the cracking of *n*-octane and compared to those obtained from H-ZSM-5 and H-ZSM-35 with the same pore architecture but different pore sizes. A high initial 1-butene conversion is observed for H-ZSM-57, while its selectivity to isobutene is much lower than that of H-ZSM-35. This trend remains almost unchanged with time on stream. Thus, the nonselective behavior of H-ZSM-57 for isobutene formation may be due not only to the presence of very strong acid sites in this zeolite as evidenced by ammonia TPD experiments, but also to its channel intersections that are large enough to allow undesired side reactions such as 1-butene dimerization followed by cracking to light olefins. By contrast, H-ZSM-57 shows considerably higher *n*-octane cracking activity than ZSM-5 known as one of the most active catalysts for this reaction. However, it is found that the poisoning of strong acid sites in H-ZSM-57 by coke formation occurs within the pores, leading to a continuous decrease in *n*-octane conversion. Such an aging feature of ZSM-57 suggests that medium-pore zeolites with intersecting channels of two different pore sizes may be less stable as acid catalysts than those with uniform pore size, due to the geometrical constraints imposed by the dual pore system, even in the case that their 10-ring pore sizes are similar to each other. © 2000 Academic Press

Key Words: **zeolite ZSM-57; synthesis; pore structure and acidity; catalytic evaluation.**

INTRODUCTION

Zeolites and molecular sieves are crystalline, microporous materials with framework structures that are based on various three-dimensional networks of TO_4 tetrahedra (T = Si, Al, P, etc.) linked to each other via doubly bridging oxygen atoms. The answer to the question about what makes them such important catalysts and separation media in the current petrochemical and refining industries can be easily found by considering the shape-selective properties of these highly porous solids directly related to the size and shape of cavities in their framework structures (1). Thus, understanding the shape-selective nature of a number of new zeolitic materials that have been continually discovered is a matter of both fundamental and industrial interest.

ZSM-57 (MFS topology) is a medium-pore, high-silica zeolite that was first described by Valyocsik and Page in 1986 (2). This synthetic zeolite belongs to the ferrierite family of zeolites and contains a two-dimensional pore system consisting of 10-ring (5.1×5.4 Å) channels in the [100] direction that intersect 8-ring (3.3×4.8 Å) channels in the [010] direction (3, 4). While the 8-ring channels in ZSM-57 are virtually identical to the analogous channels (3.5×4.8 Å) in ferrierite, the 10-ring channels are significantly larger than those (4.2×5.4 Å) in the latter zeolite. However, they are slightly smaller than the straight 10-ring (5.3×5.6 Å) and the sinusoidal 10-ring (5.1×5.5 Å) channels in ZSM-5. Therefore, the application of ZSM-57 as a shape-selective catalyst for numerous hydrocarbon conversions catalyzed by medium-pore zeolites such as ferrierite and ZSM-5 is of great practical importance. Despite its peculiar pore architecture, however, only a few studies on the physicochemical and catalytic properties of ZSM-57 have thus far been published (2, 5). Furthermore, there is little known on the crystallization conditions and the composition of the synthesis mixtures required for pure ZSM-57 formation, although this medium-pore zeolite is reported to crystallize from sodium-containing aluminosilicate gels using the doubly charged *N,N,N,N′,N′,N′*-hexaethylpentanediammonium cation as an organic structure-directing agent (SDA) (2).

In the present study we report on the synthesis and characterization of ZSM-57 and its catalytic properties for the skeletal isomerization of 1-butene to isobutene and the cracking of *n*-octane. The catalytic results are compared

[1] To whom correspondence should be addressed. E-mail: chshin@cbucc.chungbuk.ac.kr; sbhong@hyunam.tnut.ac.kr.

0021-9517/00 $35.00

to those observed with ZSM-5 and ZSM-35 (the high-silica version of ferrierite) zeolites with similar SiO_2/Al_2O_3 ratios (∼50) in order to understand the influence of zeolite pore size on the conversion of 1-butene and *n*-octane. Skeletal isomerzation of *n*-butenes has been proposed to be an attractive route for the production of isobutene, a key component in the synthesis of methyl *tert*-butyl ether (MTBE) widely used as an octane-enhancer for reformulated gasoline (6). In addition, cracking of linear paraffins like *n*-octane over medium-pore zeolites like ZSM-5 has been the subject of a number of previous studies (7).

EXPERIMENTAL

I. Synthesis

The divalent *N*,*N*,*N*,*N*′,*N*′,*N*′-hexaethylpentanediammonium (Et_6-diquat-5) cation was prepared by refluxing 1,5-dibromopentane (97%, Aldrich) with an excess of triethylamine (99%, Yakuri) in ethanol as a solvent for 4 h. The excess amine was removed by extraction with diethyl ether and recrystallizations were carried out in methanol-diethyl ether mixtures. The *N*,*N*,*N*,*N*′,*N*′,*N*′-hexaethylbutanediammonium (Et_6-diquat-4) and *N*,*N*,*N*,*N*′,*N*′,*N*′-hexaethylhexanediammonium (Et_6-diquat-6) dibromide salts were prepared by using 1,4-dibromobutane (99%, Aldrich) and 1,6-dibromohexane (96%, Aldrich) instead of 1,5-dibromopentane, respectively, with procedures similar to the Et_6-diquat-5 preparation.

Attempts to synthesize ZSM-57 were carried out using aluminosilicate gels prepared by combining NaOH (50% aqueous solution, Aldrich), organic SDA (Et_6-diquat-4, Et_6-diquat-5, or Et_6-diquat-6) prepared here, $Al(NO_3)_3 \cdot 9H_2O$ (98%, Junsei), colloidal silica (Ludox AS-40, DuPont), and deionized water. The final composition of the synthesis mixture was $3.0R \cdot x Na_2O \cdot y Al_2O_3 \cdot 30\ SiO_2 \cdot 1200 H_2O$, where *R* is the organic SDA, *x* is varied between $6.0 \leq x \leq 12.0$, and *y* is varied between $0.0 \leq y \leq 1.0$. After stirring at room temperature for 24 h, the synthesis mixture was charged into Teflon-lined 45-mL autoclaves and heated to 160°C, with or without stirring under autogenous pressure, for a given period of time. The white solid products were recovered by filtration, washed repeatedly with water, and then dried overnight at room temperature.

As-synthesized ZSM-57 was calcined in air at 550°C for 8 h to remove the organic SDA occluded. The calcined sample was then refluxed twice in NH_4NO_3 solutions for 6 h followed by calcination at 550°C for 8 h in order to ensure that the sample was completely in its proton form. For comparison, H-ZSM-35 with $SiO_2/Al_2O_3 = 54$, which is the high-silica version of ferrierite, was prepared according to procedures described elsewhere (8). In addition, two ZSM-5 zeolites with $SiO_2/Al_2O_3 = 54$ and 27 in the NH_4 form were obtained from ALSI-PENTA Zeolithe GmbH and calcined at 500°C for 6 h in order to convert them into their proton form. Here we refer to these two zeolites as H-ZSM-5(I) and H-ZSM-5(II), respectively.

II. Characterization

The phase purity was determined by powder X-ray diffraction (XRD) using a Rigaku Miniflex diffractometer with CuK_α radiation. Chemical analysis was carried out by a Jarrell-Ash Polyscan 61E inductively coupled plasma (ICP) spectrometer together with a Perkin-Elmer 5000 atomic absorption spectrophotometer. Thermogravimetric analyses (TGA) were performed in air on a TA Instruments SDT 2960 thermal analyzer, where weight loss related to the combustion of organic SDA or coke deposits formed during the reactions tested here was determined from differential thermal analyses (DTA) using the same analyzer. Approximately 15 mg of sample was used at a heating rate of 10°C min^{-1}. Crystal morphology and size were determined by a JEOL JSM-6300 scanning electron microscope. The nitrogen BET surface areas were measured on a Micromeritics ASAP 2010 analyzer.

The ^{29}Si MAS NMR spectra were measured on a Bruker DSX 400 spectrometer at a spinning rate of 12.0 kHz. The operating ^{29}Si frequency was 79.492 MHz, and the spectra were obtained with an acquisition of ca. 800 pulse transients, which were repeated with a $\pi/5$ rad pulse length of 2.0 μs and a recycle delay of 60 s. The ^1H-^{13}C CP MAS spectra at a spinning rate of 4.5 kHz were recorded on the same spectrometer at a ^{13}C frequency of 100.623 MHz with a $\pi/2$ rad pulse length of 5.0 μs, a contact time of 1 ms, and a recycle delay of 3 s. Approximately 6500 scans were accumulated. Both ^{29}Si and ^{13}C chemical shifts are referenced to TMS. The ^{27}Al MAS NMR spectra were recorded with a spinning rate of 8.0 kHz at a ^{27}Al frequency of 104.269 MHz. The spectra were obtained with an acquisition of 1024 pulse transients, which were repeated with a $\pi/20$ rad pulse length of 0.5 μs and a recycle delay of 2 s. The ^{27}Al chemical shifts are referenced to an $Al(H_2O)_6^{3+}$ solution.

Temperature-programmed desorption (TPD) of ammonia was recorded on a fixed-bed, flow-type apparatus attached to a Balzers QMS 200 quadruple mass spectrometer. Before adsorption of ammonia, ca. 0.2 g of sample were pretreated in flowing He at 550°C for 3 h. Then, pure ammonia (50 cm^3 min^{-1}) was passed over the sample at 100°C for 0.5 h. The treated sample was subsequently purged with He at the same temperature for 1 h to remove the physisorbed ammonia. Finally, TPD profiles were obtained in flowing He (200 cm^3 min^{-1}) from 80 to 650°C with a heating rate of 10°C min^{-1}.

III. Catalysis

The catalytic experiments were conducted under atmospheric pressure in a continuous-flow apparatus with a fixed-bed microreactor. Prior to the experiments, the

TABLE 1

Representative Synthesis Conditions and Results[a]

Experiment	Organic SDA used	Gel composition		Stirring (rpm)	Time (days)	Product[b]
		SiO_2/Al_2O_3	$NaOH/SiO_2$			
1	Et_6-diquat-5	60	0.6	0	21	Amorphous
2	Et_6-diquat-5	60	0.6	50	7	Mordenite + ZSM-57
3	Et_6-diquat-5	60	0.6	100	7	ZSM-57
4	Et_6-diquat-5	30	0.6	100	7	Mordenite
5	Et_6-diquat-5	120	0.6	100	7	L[c]
6	Et_6-diquat-5	∞	0.6	100	7	L[c]
7	Et_6-diquat-5	60	0.4	100	14	Amorphous
8	Et_6-diquat-5	60	0.8	100	7	P1
9	Et_6-diquat-4	60	0.6	100	5	Mordenite
10	Et_6-diquat-6	60	0.6	100	5	Mordenite

[a] The oxide composition of the synthesis mixture is $3.0R : xNa_2O : yAl_2O_3 : 30SiO_2 : 1200H_2O$, where R is organic SDA, x is varied between $6.0 \leq x \leq 12.0$, and y is varied between $0.0 \leq y \leq 1.0$. Crystallization was performed at 160°C.

[b] The phase appearing first is the major phase.

[c] Unknown, probably layered phase.

catalyst was activated under flowing He (50 cm^3 min^{-1}) at 500°C for 2 h. In the skeletal isomerization of 1-butene, a reactant stream with a He/1-butene molar ratio of 9.0 was fed into a quartz reactor containing 0.1 g of zeolite catalyst at the desired temperature. The total gas flow at the reactor inlet was kept constant at 50 cm^3 min^{-1} in all experiments. The reaction products were analyzed on-line in a Chrompack CP 9001 gas chromatograph equipped with an Al_2O_3/KCl Plot capillary column (0.53 mm × 50 m) and a flame ionization detector (FID). Conversion calculation was achieved by the methods described in our previous papers (8, 9).

n-Octane cracking was carried out in the same microreactor with 0.1 g of catalyst at atmospheric pressure. In a typical experiment, a reaction stream with a fixed partial pressure of *n*-octane (2.0 kPa) was passed over the catalyst in the temperature range 310–500°C. He was used as a carrier gas with *n*-octane as a feed, and the total gas flow was fixed to 50 cm^3 min^{-1}. The reaction products were analyzed on-line in a Chrompack CP 9001 gas chromatograph. Gaseous products with $<C_4$ were separated in a packed Porapak Q column ($\frac{1}{8}'' \times 1.8$ m) and analyzed in a thermal conductivity detector (TCD). Gaseous and liquid products with $\geq C_4$ were separated in a capillary PONA column (0.25 mm × 100 m) and analyzed in an FID. Conversion was calculated as the mole percent of *n*-octane consumed. Selectivity to a specific product *i* was calculated as the mole percent of species *i* to all products. In the absence of a catalyst, no conversion of *n*-octane was observed even at 500°C.

RESULTS AND DISCUSSION

I. Synthesis

A summary of products from synthesis mixtures with different gel compositions under the conditions described above is presented in Table 1. The original patent on the synthesis of ZSM-57 claims that this zeolite can be crystallized using Et_6-diquat-5 as an organic SDA at static or stirred conditions (2). Thus, our initial attempts to synthesize ZSM-57 were made to reproduce the reported synthesis under static conditions using an aluminosilicate gel with the optimized gel composition $3.0Et_6$-diquat-$5 \cdot 9.0Na_2O \cdot 0.5Al_2O_3 \cdot 30SiO_2 \cdot 1200H_2O$ that was adapted from the example 3 in the Mobil patent. As seen in Table 1, however, we obtained an amorphous phase even after heating at 160°C for 3 weeks. On the other hand, the synthesis using a synthesis mixture with the same composition under stirring at 50 rpm yielded a mixture of ZSM-57 and mordenite, where the latter zeolite was the major phase. When the rotation speed of the autoclaves was elevated to 100 rpm, in addition, pure ZSM-57 was obtained. This clearly shows that homogeneous mixing of the synthesis mixture at the crystallization temperature is a critical factor governing the synthesis of ZSM-57.

An unexpected result obtained from Table 1 is that the composition range leading to the successful ZSM-57 formation in the presence of Et_6-diquat-5 is very narrow. When the initial SiO_2/Al_2O_3 ratio in the synthesis mixture is decreased below 40, mordenite is the phase formed under the conditions described above. When using sodium aluminosilicate gels with $SiO_2/Al_2O_3 \geq 60$, by contrast, we obtained a phase of unknown structure and poor thermal stability (probably a layered material). We also note that crystallization of ZSM-57 depends highly on the $NaOH/SiO_2$ ratio in the gel. When the SiO_2/Al_2O_3 ratio in the synthesis mixture is fixed to 60, as seen in Table 1, the $NaOH/SiO_2$ ratio yielding pure ZSM-57 was found to be within the very narrow range (0.55–0.65). For example, the synthesis mixture with $NaOH/SiO_2 = 0.4$ remains amorphous even after crystallization at 160°C in a stirred

autoclave for 2 weeks. However, zeolite P1 with an enhanced SiO_2/Al_2O_3 ratio (ca. 8.0) compared to known isostructural materials is the phase that crystallizes from a gel with $NaOH/SiO_2 = 0.8$. The detailed synthesis and characterization of this synthetic analog of GIS-type zeolites are given elsewhere (10).

On the other hand, Schlenker *et al.* (3) have suggested that the Et_6-diquat-5 cation be arranged in an ordered manner within the 10-ring channels of ZSM-57, giving the peculiar pore architecture to the crystallizing material. This speculation was based on the fact that the length (~15 Å) of this organic cation is approximately twice the unit cell parameter (7.451 Å) in the *a*-axis of ZSM-57. In order to test whether ZSM-57 can be prepared using diquarternary ammonium cations with chain lengths different from that of Et_6-diquat-5, we have carried out the synthesis in the presence of Et_6-diquat-4 or Et_6-diquat-6 as an organic SDA. As seen in Table 1, however, neither of these two diquaternary cations directed the crystallization of ZSM-57 even under conditions where the optimized gel composition ($SiO_2/Al_2O_3 = 60$ and $NaOH/SiO_2 = 0.4$) was employed. The materials obtained were mordenites with no detectable impurities. Therefore, it is most likely that the length of the diquarternary ammonium cation is the important factor directing the synthesis of ZSM-57. However, the fact that the Et_6-diquat-5-mediated synthesis was possible only under the very narrow range of synthesis conditions described above suggests that the organic Et_6-diquat-5 cation weakly structure-directs ZSM-57.

II. Characterization

Figure 1 shows the XRD patterns of the as-synthesized and acid forms of ZSM-57 obtained from experiment 3 in Table 1. The positions and relative intensities of all the X-ray peaks from the as-synthesized sample are in good agreement with those reported in the literature (2, 5). Figure 1 also shows that the structural integrity of ZSM-57 remains intact during the initial calcination at 550°C to remove the Et_6-diquat-5 cation and the successive NH_4^+ ion exchange and calcination steps to prepare its proton form (H-ZSM-57). This can be further supported by the fact that H-ZSM-57 shows a BET surface area of 343 $m^2\ g^{-1}$ (see Table 2), revealing the high crystallinity of ZSM-57 prepared here. The scanning electron micrograph (not shown) of ZSM-57 prepared here shows the presence of small platelet-like crystallites ca. 0.5–1.0 μm wide and 0.1–0.2 μm thick, which is quite similar to the morphology reported previously (5). A combination of elemental and thermal analyses of as-synthesized ZSM-57 yields the following composition (based on 36 T-atoms per unit cell): $Na_{0.4}(Et_6\text{-diquat-}5)_{0.9}Al_{1.4}Si_{34.6}O_{72}2.5H_2O$. The unit cell formula indicates a noticeable dissimilarity between the amount of Al and the sum of Na^+ and Et_6-diquat-5 cations compensating for framework negative charges. Therefore, it is most likely that a fraction of the Et_6-diquat-5 molecules in ZSM-57 is present in the form of hydroxide or bromide to serve as a space-filling species. This can be further evidenced by the TGA/DTA curves (not shown) for as-synthesized ZSM-57 where two exothermic weight losses due to the combustion of the organic SDA appear in the temperature regions 300–500 and 500–700°C, which is quite similar to the result reported by Ernst and Weitkamp (5).

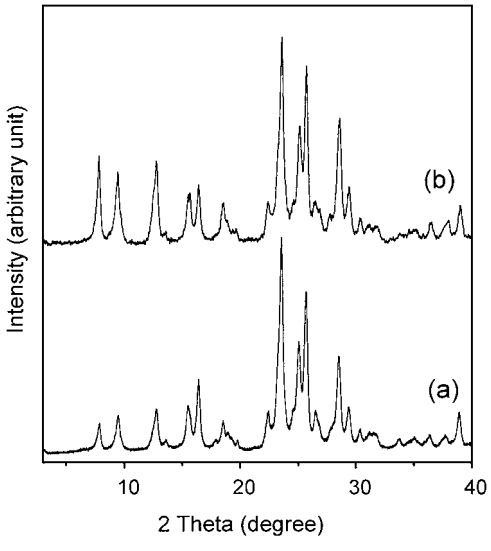

FIG. 1. Powder X-ray diffraction patterns of ZSM-57 in the (a) as-synthesized and (b) proton forms.

TABLE 2

Physical Properties of Zeolites Used in This Study

Zeolite	Structure type	Anhydrous unit cell composition	SiO_2/Al_2O_3 ratio	BET surface area[a] ($m^2\ g^{-1}$)
H-ZSM-57	MFS	$H_{1.4}Al_{1.4}Si_{34.6}O_{72}$	49	343
H-ZSM-5(I)	MFI	$H_{3.4}Al_{3.4}Si_{92.6}O_{192}$	54	333
H-ZSM-5(II)	MFI	$H_{6.6}Al_{6.6}Si_{89.4}O_{192}$	27	398
H-ZSM-35	FER	$H_{1.4}Al_{1.4}Si_{34.6}O_{72}$	49	435

[a] BET surface areas calculated from nitrogen adsorption data.

Figure 2 compares the liquid ^{13}C NMR spectrum of the Et_6-diquat-5 bromide salt with the ^1H-^{13}C CP MAS NMR spectrum of as-synthesized ZSM-57. It is clear that the organic SDA remains intact upon its occlusion into the ZSM-57 pores and has not decomposed under the synthesis conditions. When the Et_6-diquat-5 cation is trapped inside the 10-ring channels of ZSM-57, in addition, the resonances of two different types of methylene carbons bonded to the nitrogen are shifted downfield and broadened (53.5 and 57.7 ppm for Et_6-diquat-5 bromide; 55.3 and 59.0 ppm for occluded Et_6-diquat-5). This reflects the change in conformation that is imposed on Et_6-diquat-5 upon occlusion into the ZSM-57 pores. However, the resonances of the methyl

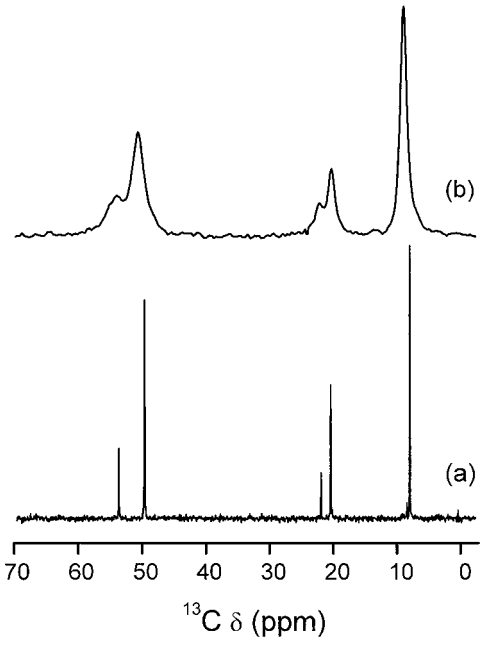

FIG. 2. ^{13}C NMR spectra of organic SDA, Et_6-diquat-5: (a) ^{13}C NMR of a $CDCl_3$ solution of the bromide form of Et_6-diquat-5 and (b) ^{1}H-^{13}C CP MAS NMR of as-synthesized ZSM-57 with Et_6-diquat-5 occluded in the pores.

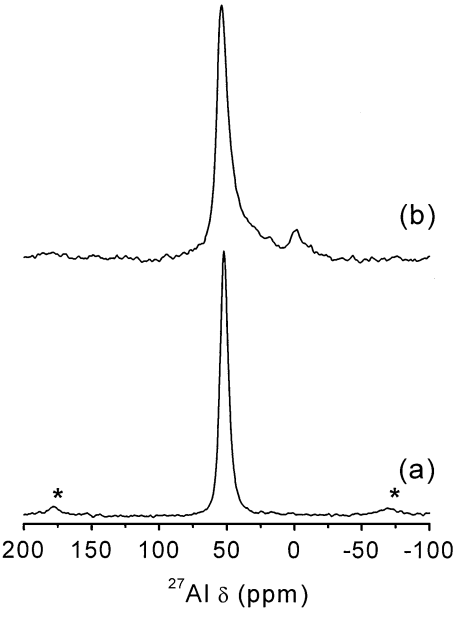

FIG. 3. ^{27}Al MAS NMR spectra of ZSM-57 in the (a) as-synthesized and (b) proton forms. Spinning side bands are marked by asterisks.

carbon in the ethyl group and of the second and third methylene carbons in the pentyl chain were found to remain essentially unchanged (8.2, 21.6, and 23.3 ppm for Et_6-diquat-5 bromide; 8.4, 21.2, 23.3 ppm for occluded Et_6-diquat-5). No shift of the resonance of the methyl carbon in the ethyl group suggests that the steric contact between the methyl carbon and the zeolite framework in the 10-ring channels is not severe. Therefore, it is most likely that the methyl carbon groups in Et_6-diquat-5 may be positioned within the intersection of 10- and 8-ring channels in ZSM-57. This can be further supported by the fact that the full width at half-maximum (fwhm) of the methyl carbon resonance at 8.4 ppm is 140 Hz, which is just half the value (280 Hz) of the resonance at 55.3 ppm assigned to the methylene carbon in the ethyl group of occluded Et_6-diquat-5.

Figure 3 shows the ^{27}Al MAS NMR spectra of the as-synthesized and acid forms of ZSM-57. Both materials exhibit a resonance at 52.3 ppm, characteristic of tetrahedral Al in the zeolite framework. However, the acid form of ZSM-57 (i.e., H-ZSM-57) also shows a line around −1 ppm, assigned to octahedral Al. This suggests that a small portion of Al has been extracted from the framework during the calcination and exchange steps. As shown in Fig. 4, on the other hand, the ^{29}Si MAS NMR spectrum of as-synthesized ZSM-57 gives one main resonance around −109 ppm, which can be attributed to $Si(OSi)_4$ species. However, an attempt to deconvolute this spectrum was unsuccessful due to the strong overlap of the lines and the possible presence of $Si(OSi)_3OH$ species in the chemical shift range 102–104 ppm (11). Figure 4 also shows that the subsequent calcination and exchange treatments caused no significant changes in the ^{29}Si MAS NMR spectrum of ZSM-57, while some dealumination may have occurred according to the ^{27}Al MAS NMR results.

Figure 5 shows the NH_3 TPD profiles obtained from H-ZSM-57, H-ZSM-5(I), and H-ZSM-35 zeolites. All the TPD profiles in Fig. 5 are characterized by two desorption peaks

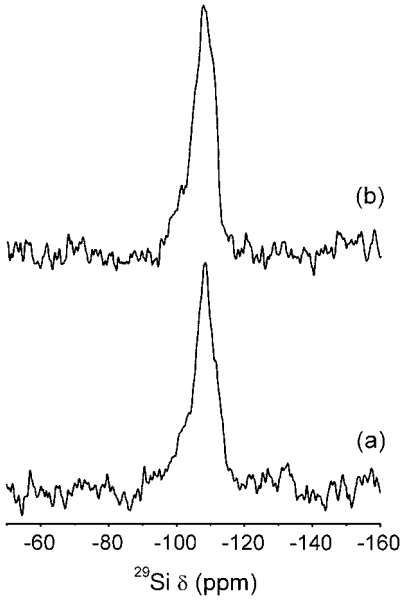

FIG. 4. ^{29}Si MAS NMR spectra of ZSM-57 in the (a) as-synthesized and (b) proton forms.

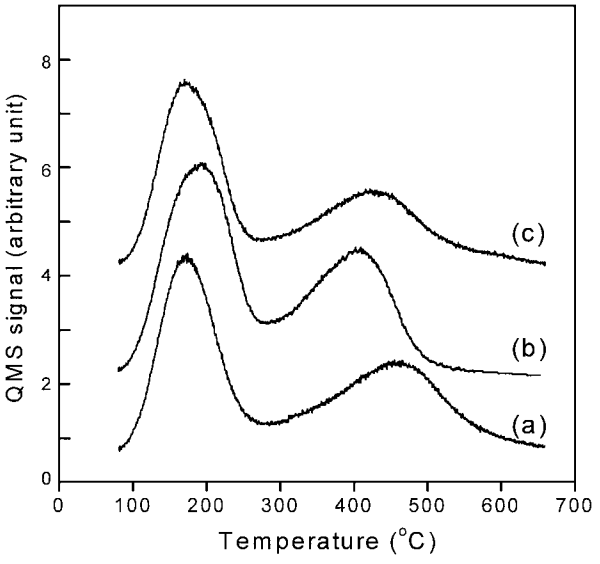

FIG. 5. NH_3 TPD profiles from (a) H-ZSM-57, (b) H-ZSM-5(I), and (c) H-ZSM-35 zeolites.

with maxima in the temperature regions 170–200 and 410–460°C, which can be assigned to NH_3 desorption from weak and strong acid sites, respectively. As expected from the similarity in the SiO_2/Al_2O_3 ratios (Table 2), the total area of NH_3 desorption (i.e., the density of acid sites) is comparable for the three zeolites. However, the distribution of acid strengths appears to be different. Compared to H-ZSM-5(I), for example, the high-temperature desorption peak from H-ZSM-57 is somewhat broader and located at a higher temperature (maximum around 460°C). This indicates that the strong acid sites in ZSM-57 possess a higher strength and a broader strength distribution than those in H-ZSM-5(I), which can be partly attributed to extraframework Al species detected by ^{27}Al MAS NMR (Fig. 3). On the other hand, extensive IR investigations into the acidic properties of zeolites have repeatedly shown that the acidity associated with framework Al atoms is stronger in H-ZSM-5 than in ferrierite or its high-silica analog, i.e., ZSM-35 (12–14). However, the TPD results in Fig. 5 reveal that the temperature maximum (420°C) of the high-temperature desorption peak from H-ZSM-35 is slightly higher than that (ca. 410°C) from H-ZSM-5(I), as reported in previous studies (8, 14). This can be rationalized by considering that the extent of readsorption from one strong acid site to another strong acid site during the TPD experiment, yielding the shift of the desorption peak to the higher temperature region (15), may be more severe in H-ZSM-35 than in H-ZSM-5(I), due to the smaller pore size of the former zeolite.

III. Catalysis

Figure 6 shows 1-butene conversion and selectivity to isobutene as a function of time on stream in skeletal isomerization on H-ZSM-57, H-ZSM-5(I), and H-ZSM-35 zeolites at 400°C and 10.1 kPa 1-butene in the feed. It is well established that ferrierite, known as the best catalyst among the zeolites tested so far, exhibits high selectivity to isobutene only after partial deactivation by coke deposition within its pores (9, 14, 16). In order to avoid the secondary effect of coke on the selectivity to isobutene, therefore, we have considered here the results obtained at 5 min on stream as the intrinsic activities of the zeolites studied here (17). When H-ZSM-57 is compared with H-ZSM-35 isostructural to ferrierite under the same reaction conditions, the former zeolite gives a higher initial 1-butene conversion

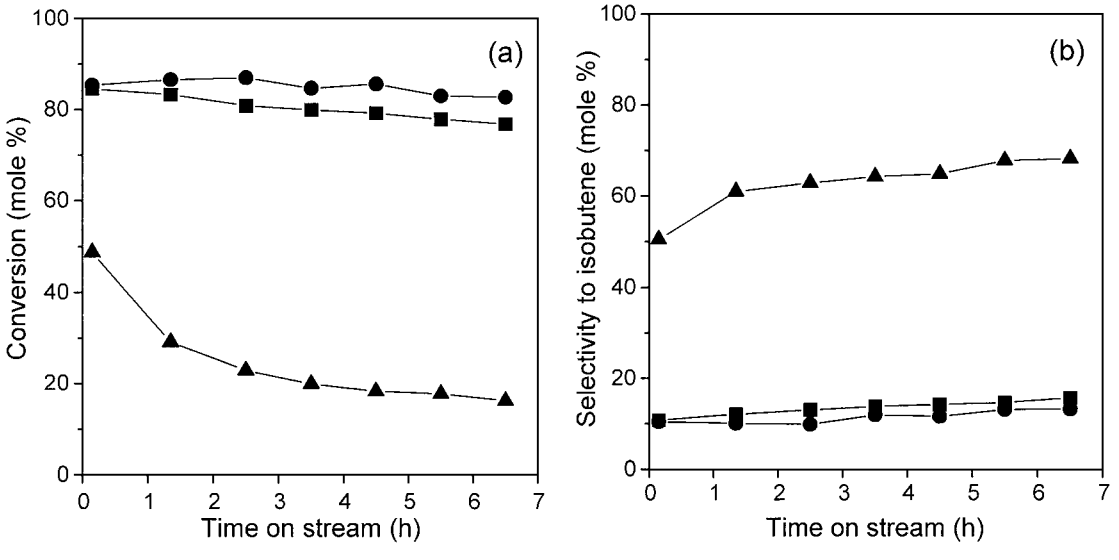

FIG. 6. Evolution with time on stream of (a) 1-butene conversion and (b) selectivity to isobutene for H-ZSM-57 (squares), H-ZSM-5(I) (circles), and H-ZSM-35 (triangles) at 400°C and 10.1 kPa 1-butene pressure.

(84 aganist 49%). As seen in Fig. 6, however, H-ZSM-57 produces a much higher amount of by-products (mainly propene and pentenes) than H-ZSM-35 from the beginning of the reaction, revealing a higher activity for the dimerization of butenes to octenes followed by cracking. As a result, the initial selectivity (15%) to isobutene on H-ZSM-57 is much lower than that (51%) obtained on H-ZSM-35. This can be attributed to the presence of very strong acid sites in H-ZSM-57, as observed from the NH_3 TPD profiles in Fig. 5.

Figure 6 also shows that H-ZSM-35 becomes more selective for isobutene formation with increasing time on stream, which corresponds to the trend observed in previous studies (9, 16). However, the selectivity to isobutene on H-ZSM-57 remains almost unchanged over the period of time studied here, which is essentially the same as the behavior of H-ZSM-5(I). While the pore system in both ZSM-57 and ZSM-35 consists of two perpendicular intersecting 10- and 8-ring channels, the 10-ring channels are significantly larger in the former zeolite (5.1×5.4 Å versus 4.2×5.4 Å). Therefore, it is clear that the free diameter at the H-ZSM-57 intersection must be much larger than that at the H-ZSM-35 intersection, leading to a more efficient accommodation of two *n*-butenes for side reactions such as their dimerization followed by cracking to light hydrocarbons. This led us to believe that the nonselective behavior of H-ZSM-57 for isobutene formation may originate from its large intersected channels, as well as from the presence of very strong acid sites in this zeolite. The amounts of coke deposited on zeolite catalysts after the skeletal isomerization of 1-butene at 450°C for 6 h have been determined by TGA/DTA and are given in Table 3. No significant differences in the amount (7–8%) of coke formed are observed for H-ZSM-35 and H-ZSM-57 with the same pore system. This suggests that the difference (0.9 Å) in the shortest 10-ring pore dimensions of ZSM-35 and ZSM-57 are not large enough to influence the rate of coke formation on these zeolites.

TABLE 3

Amounts of Coke Deposits Formed on H-ZSM-57, H-ZSM-5, and H-ZSM-35 Zeolite Catalysts during the 1-Butene Skeletal Isomerization and *n*-Octane Cracking[a]

Zeolite	SiO_2/Al_2O_3 ratio	Amount (wt%) of coke deposited[b]	
		1-Butene skeletal isomerization	*n*-Octane cracking
H-ZSM-57	49	7.9	7.2
H-ZSM-5(I)	54	5.1	5.8
H-ZSM-35	49	7.0	5.2

[a] After 6 h on stream. The reaction temperatures for 1-butene skeletal isomerization and *n*-octane cracking are 400 and 500°C, respectively. The other conditions for each reaction are the same as those stated in the text.

[b] Determined from TGA/DTA.

TABLE 4

Conversion and Product Distribution from Catalytic Cracking of *n*-Octane on H-ZSM-57, H-ZSM-5, and H-ZSM-35 Zeolite Catalysts at 500°C[a]

Catalyst	H-ZSM-57	H-ZSM-5(I)	H-ZSM-5(II)	H-ZSM-35
Conversion (mol%)	87.7	60.1	84.3	12.6
Selectivity (mol%) to				
Methane	2.2	1.4	3.2	—
Ethane	6.8	7.6	7.3	—
Ethylene	28.8	21.9	28.8	19.4
Propane	14.3	13.3	14.8	13.4
Propylene	28.6	30.9	25.6	30.9
n-Butane	5.7	7.2	5.5	6.2
Isobutane	1.4	0.7	1.6	1.5
1-Butene	4.5	6.2	4.2	10.4
cis-2-Butene	1.8	3.0	1.7	4.6
trans-2-Butene	1.4	2.1	1.3	3.4
n-Pentane	0.1	0.3	0.1	0.9
2-Methylbutane	—	—	0.1	0.5
1-Pentene	0.1	0.2	0.2	1.1
2-Pentene	1.5	3.0	1.7	3.8
cis-2-Pentene	0.1	0.1	—	—
trans-2-Pentene	0.3	0.6	0.3	1.3
n-Hexane	0.1	0.4	0.2	1.4
2-Methylpentane	0.1	0.2	0.1	—
Benzene	0.6	0.3	0.9	—
Toluene	1.1	0.6	1.8	1.2
p-Xylene	0.5	—	0.6	—

[a] Data are reported as the values of 500 s on stream at a total gas flow of 50 cm^3 min^{-1}.

Table 4 lists the conversions and product distributions from the catalytic cracking of *n*-octane on H-ZSM-57, H-ZSM-5(I), and H-ZSM-35 zeolites measured at 500°C, 2.0 kPa *n*-octane pressure in the feed, and 500 s time on stream. For comparison, the catalytic results from ZSM-5(II) with a higher Al content are also given in Table 4. These data reveal that the *n*-octane conversion (88%) on H-ZSM-57 is much higher than that (13%) on H-ZSM-35. This is not unexpected because both the strength and amount of strong acid sites are higher in H-ZSM-57 than in H-ZSM-35 as determined by NH_3 TPD experiments (Fig. 6). In addition, it appears that the spatial constraints for the free diffusion of *n*-octane molecules in the ZSM-57 pores are not so severe as those of the ZSM-35 pores. Due to its exceptional activity and stability, on the other hand, H-ZSM-5 with two intersecting 10-ring channels serves as a prime example of the uniqueness of medium-pore zeolites in the cracking of linear paraffins (1, 18, 19). As seen in Table 4, H-ZSM-5(I) yields an *n*-octane conversion of 60% under conditions given above. When H-ZSM-57 is compared with H-ZSM-5 with a similar SiO_2/Al_2O_3 ratio, therefore, the former zeolite exhibts a considerably higher *n*-octane conversion. We note that the *n*-octane conversion on H-ZSM-57 is comparable to that (84%) observed

for H-ZSM-5(II) with a higher Al content. The catalytic data in Table 4 also show that ethylene and propylene are the two most dominant products observed for all zeolite catalysts studied here. The other major products include ethane, propane, *n*-butane, and butenes. Minor products comprise methane, isobutane, *n*-pentane, pentenes, etc. These product distributions are quite different from those for H-ZSM-5 with $SiO_2/Al_2O_3 = 14.2$ reported by Smirniotis and Ruckenstein (20), where aromatic hydrocarbons such as benzene, xylenes, and toluene are major products. The discrepancy with our results appears to be due to differences in the reaction conditions (mainly contact time) employed in the respective catalytic runs.

Another interesting result obtained from Table 4 is that the ratio of propylene to ethylene is approximately unity for H-ZSM-57, but is shifted to larger values for H-ZSM-5(I) and H-ZSM-35. This indicates a higher secondary cracking activity of H-ZSM-57, which is in good agreement with the NH_3 TPD results. In order to investigate the effect of reaction temperature on product selectivities, on the other hand, we have carried out the *n*-octane cracking reaction on H-ZSM-57 in the temperature region 310–500°C. In general, selectivites to ethylene and propylene become higher with increasing reaction temperature. However, the opposite was observed for the selectivities to longer hydrocarbons, mainly *n*-butane and butenes. This suggests that the extent of secondary cracking activity of H-ZSM-57 becomes larger at a higher reaction temperature. A similar trend was found on the other two zeolites studied here.

Figure 7 shows *n*-octane conversion and selectivities to ethylene and propylene as a function of time on stream in *n*-octane cracking on H-ZSM-57, H-ZSM-5(I), and H-ZSM-35 zeolites at 500°C and 2.0 kPa *n*-octane pressure in the feed. It can be seen that *n*-octane conversions on H-ZSM-5(I), and H-ZSM-35 remain almost constant during the period of 6 h on stream, while a continuous decrease in *n*-octane conversion is observed for H-ZSM-57. This indicates that H-ZSM-57 deactivates continuously during the *n*-octane cracking, unlike H-ZSM-5(I) and H-ZSM-35. A trend of decreasing *n*-octane conversion on H-ZSM-57 with time on stream was found to remain unchanged over the temperature range (310–500°C) studied here, although the extent of this decrease in conversion is smaller at lower temperatures. In any case, however, the *n*-octane conversion on H-ZSM-57 at a final time on stream is still considerably higher than that on H-ZSM-5 with a similar SiO_2/Al_2O_3 ratio, revealing a higher activity of H-ZSM-57 for the cracking of *n*-octane. As seen in Fig. 7, for example, H-ZSM-57 and H-ZSM-5(I) exhibit *n*-octane conversions of 75 and 58% at 6 h on stream and 500°C, respectively. We also note that no significant changes in the product distribution with time on stream are observed for H-ZSM-5(I) and H-ZSM-35, while the distribution of cracking products on H-ZSM-57 is shifted to higher carbon numbers. As a result, the amount of propylene produced becomes higher at higher times on stream, and the opposite is observed for ethylene formation. The TGA/DTA results in Table 3 reveal that after the *n*-octane cracking at 500°C for 6 h, a higher amount of coke is formed on H-ZSM-57 than on H-ZSM-5(I), despite the similarity in the pore sizes of the 10-ring channels in these two zeolites. Therefore, it is clear that the aging feature observed for H-ZSM-57 during 6 h on stream must be due to the continuous poisoning of strong acid sites by coke deposited within the pores. Based on the overall results of this study, in addition, we conclude that the pore structure of H-ZSM-57 with intersecting 10- and 8-ring channels of

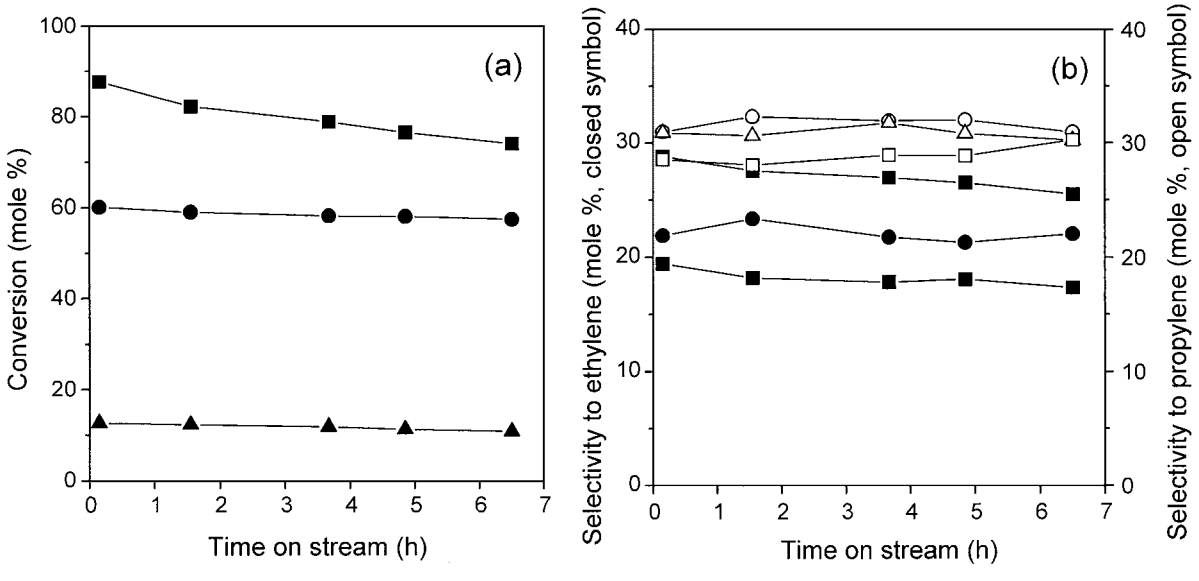

FIG. 7. Evolution with time on stream of (a) *n*-octane conversion and (b) selectivities to ethylene and propylene for H-ZSM-57 (squares), H-ZSM-5(I) (circles), and H-ZSM-35 (triangles) at 500°C and 2.0 kPa *n*-octane pressure.

two different pore sizes, rather than its very strong acidity, may be responsible for the higher coke forming tendency compared to H-ZSM-5 with the uniform pore size, although the 10-ring channels in both zeolites have similar pore sizes. This led us to believe that H-ZSM-57 is less stable than H-ZSM-5 as an acidic catalyst, despite its higher activity for the cracking of *n*-octane. It is well established that the pore structure of zeolites exerts a very large effect on the rate of coke formation in a number of acid-catalyzed reactions (1). When the 10-ring pore sizes of zeolites studied here are compared to one another, on the other hand, the diffusion of *n*-octane molecules may be less favorable in H-ZSM-35 than in H-ZSM-5 or H-ZSM-57. Thus, the stable but low activity observed for H-ZSM-35 in Fig. 7 can be rationalized by considering that the external acid sites on the H-ZSM-35 crystals, on which catalysis is not influenced by shape selectivity, may contribute mainly to the cracking of *n*-octane. This can be further supported by the slightly smaller amount of coke deposited on H-ZSM-35 during 6 h on stream as compared with H-ZSM-5 (see Table 3).

Finally, we have treated the H-ZSM-57 sample after 6 h of *n*-octane cracking in flowing air at 500°C for 1 h in order to check whether the partially deactivated H-ZSM-57 can be regenerated. It was found that the used H-ZSM-57 zeolite regained its initial activity, since successive experiments under identical conditions gave almost the same conversion and product selectivities compared to those from the fresh H-ZSM-57 catalyst. Therefore, it appears that most of the carbonaceous deposits formed on H-ZSM-57 may be aliphatic in nature, since coke with properties of polycyclic aromatics is diffcult to be removed from the zeolite under the conditions given above. However, it should be noted that the ^{13}C MAS NMR spectrum (not shown) of ZSM-57 after *n*-octane cracking at 500°C for 6 h gave three main resonances at 27.5, 37.0, and 44.2 ppm, together with two additional low-intensity resonances around 145 and 186 ppm. This clearly shows formation of aliphatic and, to a lesser extent, aromatic carbonaceous residues in ZSM-57 (21).

CONCLUSIONS

Zeolite ZSM-57 with the intersecting 10- and 8-ring pore system was found to crystallize over a very narrow range of SiO_2/Al_2O_3 and $NaOH/SiO_2$ ratios in the presence of sodium and *N*,*N*,*N*,*N*′,*N*′,*N*′-hexaethylpentanediammonium cations. The physico-chemical properties of ZSM-57 prepared here are investigated by XRD, elemental analyses, multinuclear solid-state NMR, and ammonia TPD. The characterization results reveal the presence of very strong acid sites in H-ZSM-57. The skeletal isomerization of 1-butene to isobutene and the cracking of *n*-octane are studied on H-ZSM-57. When compared to H-ZSM-35 with a similar SiO_2/Al_2O_3 ratio, a high 1-butene conversion is observed for H-ZSM-57 while its selectivity to isobutene is much lower than for H-ZSM-35. In the cracking of *n*-octane, on the other hand, H-ZSM-57 shows considerably higher cracking activity than H-ZSM-5. Despite the similarity in the 10-ring pore sizes of H-ZSM-5 and H-ZSM-57, however, a continuous deactivation during the cracking reaction by coke formation is observed for the latter zeolite. The geometrical constraints of H-ZSM-57 imposed by two intersecting 10- and 8-ring channels with different pore sizes, rather than its strong acidity, appear to be the main reason for the high coke forming propensity, compared to H-ZSM-5, in acid-catalyzed reactions.

ACKNOWLEDGMENTS

Financial support for this work was provided by the Korea Energy Management Corporation R&D Management Center for Energy and Resources and the Korea Science and Engineering Foundation through the Advanced Materials Research Center for a Better Environment at Taejon National University of Technology.

REFERENCES

1. Chen, N. Y., Garwood, W. E., and Dwyer, F. G., "Shape Selective Catalysis in Industrial Applications." Dekker, New York, 1989.
2. Valyocsik, E. W., and Page, N. M., European patent 0174 121 A2 (1986).
3. Schlenker, J. L., Higgins, J. B., and Valyocsik, E. W., *Zeolites* **10**, 293 (1990).
4. Meier, W. M., Olson, D. H., and Baerlocher, Ch., "Atlas of Zeolite Structure Types," 4th ed. Elsevier, London, 1996.
5. Ernst, S., and Weitkamp, J., *Stud. Surf. Sci. Catal.* **65**, 645 (1991).
6. Butler, A. C., and Nicolaides, C. P., *Catal. Today* **18**, 443 (1993).
7. Chen, N. Y., Degnan, T. F., Jr., and Smith, C. M., "Molecular Transport and Reaction in Zeolites." VCH, New York, 1994.
8. Seo, G., Jeong, H. S., Hong, S. B., and Uh, Y. S., *Catal. Lett.* **36**, 249 (1996).
9. Seo, G., Jeong, H. S., Jang, D.-L., Cho, D. L., and Hong, S. B., *Catal. Lett.* **41**, 189 (1996).
10. Paik, W. C., Shin, C.-H., and Hong, S. B., *Chem. Commun.* 1609 (2000).
11. Engelhardt, G., and Michel, D., "High-Resolution Solid-State NMR of Silicates and Zeolites." Wiley, Chichester, 1987.
12. Jacobs, P. A., and von Ballmoos, R., *J. Phys. Chem.* **86**, 3050 (1982).
13. Zholobenko, V. L., Lukyanov, D. B., Dwyer, J., and Smith, W. J., *J. Phys. Chem.* **102**, 2715 (1998).
14. Xu, W.-Q., Yin, Y.-G., Suib, S. L., Edwards, J. C., and O'Young, C.-L., *J. Phys. Chem.* **99**, 9443 (1995).
15. Farneth, W. E., and Gorte, R. J., *Chem. Rev.* **95**, 615 (1995).
16. Guisnet, M., Andy, P., Gnep, N. S., Travers, C., and Benazzi, E., *J. Chem. Soc. Chem. Commun.* 1685 (1995).
17. Meriaudeau, P., Vu Tuan, A., Le Hung, N., and Szabo, G., *Catal. Lett.* **47**, 71 (1997).
18. Haag, W. O., Lago, R. M., and Weisz, P. B., *Nature* **309**, 589 (1984).
19. Watson, B. A., Klein, M. T., and Harding, R. H., *Ind. Eng. Chem. Res.* **35**, 1506 (1996).
20. Smirniotis, P. G., and Ruckenstein, E., *Ind. Eng. Chem. Res.* **33**, 800 (1994).
21. Karge, H. G., *Stud. Surf. Sci. Catal.* **58**, 531 (1991).